PNAS
www.pnas.org

Supplementary Information for

Antibiotic resistance and host immune evasion in *Staphylococcus aureus* mediated by a metabolic adaptation

Jhih-Hang Jiang, Md Saruar Bhuiyan, Hsin-Hui Shen, David R. Cameron, Thusitha W. T. Rupasinghe, Chun-Ming Wu, Anton P. Le Brun, Xenia Kostoulias, Carmen Domene, Alex J. Fulcher, Malcolm J. McConville, Benjamin P. Howden, Graham J. Lieschke and Anton Y. Peleg

Anton Y. Peleg
Email: anton.peleg@monash.edu

This PDF file includes:

SI Materials and Methods
Figs. S1 to S8
Tables S1 to S10
References for SI reference citations

www.pnas.org/cgi/doi/10.1073/pnas.1812066116

SI Materials and Methods

Media and reagents

Bacterial strains, plasmids, and oligonucleotides used in this study are described in Table S6. *S. aureus* cells were cultured at 37 ºC in heart infusion broth (HI) (Oxoid) with constant shaking. *Escherichia coli* cells were cultured at 37 ºC in Luria-Bertani brothwith constant shaking. Chloramphenicol (Cm) and anhydrotetracycline (aTc, Sigma Aldrich) were used at a final concentration of 10μg/ml and 1μg/ml respectively as required. Synthetic lysyl-phosphatidylglycerol (18:1), phosphatidylglycerol (18:1) and cardiolipin (18:1) were purchased from Avanti Polar Lipids, Inc.

Genetic manipulation

The vector pIMAY and the *E. coli* strain DC10B were used to genetically manipulate *S. aureus* isolate A8819 following the published protocol (1). DNA fragments were amplified from genomic DNA using primer pairs AP515/AP382 or AP383/AP529 followed by annealing PCR using primers AP515/AP529. A new *Eco*RV restriction site close to the nucleotide mutation of interest was introduced without altering the protein sequence to differentiate mutants from the parental strain. Colony PCR with the primer pair AP352/AP353 was used to detect pIMAY in *E. coli* and *S. aureus* transformants (1). Point mutations of *cls2* were confirmed by DNA sequencing using AP515, AP517 and AP529.

Daptomycin susceptibility testing

Daptomycin was provided by Cubist Pharmaceuticals (Lexington, MA) and broth microdilution MIC testing was performed based on guidelines by the Clinical and laboratory standards institute (CLSI). E-tests (Biomerieux) were also conducted according to manufacturer's recommendations. A minimum of three independent experiments were performed. Daptomycin MIC > 1 μg/ml is officially termed daptomycin-nonsusceptible (2), but was termed daptomycin resistant throughout the manuscript for clarity.

Time-kill assays were performed with an initial bacterial inoculum of 10^6 CFU/ml in Mueller-Hinton broth (MHB) supplemented with 50 mg/litre calcium and daptomycin at

concentrations ranging from 0 to 6 μg/ml. Viable bacterial cells were determined after 0, 4, 8, 12, 16 and 24 h of daptomycin exposure. Comparisons between time-kill curves were performed using the area under curve (AUC) for each strain and were calculated using the trapezoidal rule and statistically compared using Analysis of variance (ANOVA) (3). The detection limit (1 $\log_{10}$ CFU/ml) was set as the baseline for AUC calculation. To analyse if further daptomycin resistance and additional adaptation occurred under daptomycin exposure, viable staphylococcal cells were collected from the plates for further analysis. At least three colonies grown on the plates at each time point from the time-kill analysis were randomly picked, mixed and resuspended in MHB for daptomycin susceptibility testing. For wild-type cells at the 24 hour daptomycin treatment time point, only one colony was found after three experiments and the MIC of this colony was shown in Fig 1C.

Lipid analysis by mass spectrometry

Lipids were extracted at different stages throughout the bacterial growth phase (exponential to stationary) and were analysed using thin-layer chromatography following the published protocol (4). Dried lipids were processed according to published protocol (5) and lipid species from each lipid class were identified using positive ion mode precursor ion for PG, neutral loss scanning for L-PG, and negative ion mode full scan for CL. Identified lipid species were quantified using multiple reaction monitoring (MRM). The concentration of each lipid species in the samples was determined by using the regression model to convert normalized peak area to lipid concentration.

For measurement of *de novo* phospholipid biosynthesis, the metabolic labelling was initiated by the addition of glycerol or [^{13}C]-glycerol (Sigma-Aldrich) to 1 mM after bacterial growth from optical density 600nm of 0.4 for 30 minutes at 37 ºC. Lipids were extracted from the cells after 0, 15 and 60 minutes incubation. For the identification of ^{13}C-PG, precursor 189 scan was used to identify ^{13}C-glycerol incorporated into the backbone whilst precursor 192 scan was used to identify ^{13}C-glycerol incorporated into either the head group or both the head group and backbone. For the identification of ^{13}C- LPG species, neutral loss of 300 scan was used to identify ^{13}C-glycerol incorporated into the backbone

whilst neutral loss of 303 scan was used to identify ^{13}C-glycerol incorporated into the head group or both the head group and backbone. ^{13}C-glycerol incorporation into CL species was identified based on the mass shift of +3, +6 and +9 using the full scan. Data collected for lipid composition of PG, CL and L-PG with ^{13}C-glycerol incorporation was analysed by the open source statistical analysis software, Metaboanalyst (http://www.metaboanalyst.ca).

S. aureus bilayer membrane formation

Deposition of the model membrane on the top of a SiO_2 surface was performed using a custom built Langmuir-Blodgett trough (Nima Technology, Conventry, UK) following published Langmuir–Blodgett (LB) and Langmuir–Schaefer (LS) procedures (6). Briefly, lipids dissolved in chloroform were deposited onto a water surface with 5mM $CaCl_2$ cooled to 10°C. The membrane models were deposited onto the SiO_2 surfaces in two stages: firstly, the inner leaflet of the bilayer was deposited using LB deposition followed by outer leaflet formation using the LS procedure. The silicon wafer with deposited bilayer was clamped into an aluminum holder with silicon backing plate and an inlet and outlet tube to allow for the exchange of HEPES buffers (5mM $CaCl_2$, 150mM NaCl, 10mM HEPES, pH 7.4) in D_2O or H_2O. Synthetic PG (18:1), CL (18:1) and L-PG (18:1) were mixed at the molar ratios of 69:12:19 and 23:60:17 to create A8819 and A8819$_{Cls2T33N}$ symmetric membrane bilayers, respectively.

Neutron reflectometry (NR)

Specular neutron reflection at solid-liquid interface was carried out on the Platypus time-of-flight neutron reflectometer (7) at the OPAL 20 MW Multi-purpose Research Reactor, Lucas Heights, Australia. The instrument uses a white neutron beam of ~2.8 Å to ~18 Å neutrons through facing the neutron cold source. Neutron pulses of 24 Hz were generated using rotating discs set in the medium resolution mode ($\Delta\lambda/\lambda$ ~ 4 %). Data was collected on a 2-dimensional ^{3}He detector. Reflectivity was collected on each surface at two incident angles of 0.85 and 3.5 degrees with an illuminated footprint of 60 mm. Measurements were performed in H_2O and D_2O. Data was reduced using the SLIM in-house software (8), which stiches the reflectivity from each incident angle together at the appropriate overlap region

to generate a complete profile, re-bins the data to instrument resolution, and subtracts background. The final reflectivity (reflected intensity / incident intensity) is presented as a function of momentum transfer, Q, defined as: $Q = 4\pi \sin\theta / \lambda$, where θ is the angle of incidence and λ is the neutron wavelength.

Analysis of the NR profiles was performed using the MOTOFIT analysis software (9). Briefly, the layer was divided into several sublayers and then a characteristic matrix was evaluated for each sublayer, from which the whole reflectivity was calculated exactly. The same layer with multiple datasets with different isotopic contrasts was fitted simultaneously until the satisfactory fit was obtained (smallest χ^2 value in the genetic algorithm). All models included a 13 Å oxide layer on the surface of the silicon wafers. The model of the two head groups with the tail region in between was used to characterise the thickness of the membrane bilayer. Finally, daptomycin penetration into the membrane and assembly on the top of the membrane was evaluated.

The best-fit model from Motofit gave information about the thickness, density and roughness of each layer. When a layer was composed of just two components, a chemical species or its fragment *s* and water *w*, the scattering length density was given by:

$$\rho_{layer} = \phi\rho_s + (1-\phi)\rho_w$$

where ρ_w and ρ_s are the scattering length densities of the two components, respectively and ϕ is the volume fraction of species s in the layer. If more than one chemical species was present, then ρ_s was determined by the volume fraction of each species in the layer.

Estimates of parameter uncertainties were obtained through using a Monte Carlo resampling procedure on the best data fits obtained using MOTOFIT (10, 11). The uncertainties were obtained by generating 1008 synthetic data sets that were produced by applying random Gaussian weighted deviations from the data based on the counting statistics of the real data. The synthetic data sets were then analysed in the same way as real data, outputting 1008 variations for each parameter that was fitted. The fits to the synthetic data were analysed by producing a frequency plot of the fitted values. The distribution of each parameter was statistically analysed with the parameter value being the

midpoint of the 95 % confidence interval and the error defined as twice the standard deviation of the distribution.

Small angle neuron scattering (SANS)

Synthetic PG, CL and L-PG were dissolved in chloroform and mixed at the molar ratios of 69:12:19 and 23:60:17 for A8819 and $A8819_{Cls2T33N}$ membranes respectively. The lipid mixtures were dried under nitrogen and resuspended in HEPES buffer (5mM $CaCl_2$, 150mM NaCl, 10mM HEPES, pH 7.4) with D_2O using a water bath sonicator. Daptomycin was added to the membrane suspension and the mixtures were transferred to Hellma cuvettes (Hellma Analytics, Germany). The samples were measured using the small-angle neutron scattering instrument, Quokka (12), at ANSTO with the configuration performed over a Q range of ~0.02-0.21 $Å^{-1}$ where q is the magnitude of the scattering vector defined as $Q = 4\pi/\lambda \cdot sin\theta$, with λ=5 Å, Δλ/λ= 10% resolution and the scattering angle 2θ, providing a length scale of 3-31.4 nm. The distances of source-to-sample (L1) and sample-to-detector (L2) were 4 meters, with source and sample apertures of 50 mm and 5 mm diameter respectively.

The data were reduced using SANS reduction macros developed at the National Institute of Standards and Technology Center for Neutron Research (USA) within Igor software package modified for the Quokka instrument, and transformed to absolute scale by the use of an attenuated direct beam transmission measurement (13, 14). For the deduction of daptomycin-bound membrane structure, the data obtained from HEPES buffer in D_2O alone was used for background subtraction using the Igor pro package (13). The spectra were analyzed using in-built algorithms within the SASview package 4.1 (http://www.sasview.org/). The standard core-shell and hollow-cylinder models were utilized for the fitting of the daptomycin micelles to calculate the radius of the core (Rc) and the thickness of the micelle (Rm) (15).

Zebrafish strains, maintenance and leukocyte enumeration

Wild-type Tübingen and Tg(*lyz*:DsRed)^{nz50} zebrafish (16) embryos were maintained in the Monash University Fish Core facility according to standard protocols (17). Zebrafish

embryos (48 hours post fertilization) were infected in either the somite tissue of the tail or otic vesicles with *S. aureus* wild-type and mutant strains following a previous published protocol (17). For the bacterial burden assays, *S. aureus* strains carrying pALC2084 (18) were used for infection in the somite tissue of the tail, and zebrafish embryos were homogenized at indicated time points followed by plating on HI agar supplemented with Cm to detect live *S. aureus* cells. For microscopy, zebrafish were immobilized in 1% low melting temperature agar. Routine bright field and fluorescence imaging was performed using a Zeiss Lumar V12 stereo dissecting microscope with an AxioCam MRm camera running AxioVision 4.8 software. Neutrophil counts were scored in a blinded fashion at 6 hours following infection or inoculation and images were analyzed using Image J software. On the basis of a power analysis, a sample size of $n \geq 10$ per group was used to provide 95% confidence that a significant difference in neutrophil recruitment could be detected. The injection of materials into zebrafish was performed without randomization and was completed with approval of the Monash University Animal Ethics Committee.

***In vitro* Transwell chemotaxis assay**

Human venous blood was collected from healthy volunteers for this study with the approval of the Monash University Human Research Ethics Committee. Neutrophils were isolated using EasySep^{TM} Direct Human Neutrophil Isolation Kit (STEMCELL TECHNOLOGIES) according to the manufacturer's protocol. Chemotaxis assays were performed using 96-well HTS Transwell system with permeable supports (3 μm pore size; Corning Inc.) following the published protocol (19). A 100 μl suspension of 2.5×10^5 neutrophils in Hanks' balanced salt solution (HBSS) was added to each well of the upper filter plate. A 150 μl suspension of bacterial cells (4.5×10^6 CFU) was added to each of the lower wells.

Liposome preparation

Staphylococcal PG or CL were extracted from TLC plates using chloroform/methanol/water (5:5:1) followed by centrifugation. Liposomes were prepared following the established protocol (20). Briefly, the lower phase was dried under nitrogen, weighed, dissolved in chloroform/methanol (2:1) and then evaporated with nitrogen to produce a lipid film on round-bottom glass tubes. Lipid films were further dried under

vacuum for 16 hours and then dispersed in PBS to reach 1 mg/ml with vigorous shaking. The resulting lipid suspension was extruded through a 100 nm polycarbonate filter 12 times and used within 24 hours.

Quantitative reverse transcription PCR (qRT-PCR)

RNA was extracted from *S. aureus* cells grown to exponential phase (OD ~ 0.5). Briefly, 4 ml of cells was added to 2 ml of RNA later (QIAGEN) then incubated at room temperature for at 10 minutes. Cells were disrupted by two 30-second cycles of bead beading (6500 rpm). Total RNA was harvested using the RNesy kit (QIAGEN) with 2 on column digestions with DNAse (QIAGEN). Complementary DNA (cDNA) was synthesized using Superscript III reverse transcriptase (Life Technologies) and diluted to 1:10 or 1:100 for qPCR. qPCR was performed using SYBR green (Life Technologies) in triplicate with primers AP85/AP86 and AP151/AP152 for *cls2* and 16S rRNA respectively (Table S10). Expression of *cls2* was normalized to 16S rRNA and expression changes were determined using the $2^{-\Delta\Delta C}$T method.

Western immunoblot analysis

S. aureus cells were grown to exponential phase and the cells were collected using centrifugation followed by treatment with 0.5 mg/ml lysostaphin and 0.1 mg/ml lysozyme in phosphate-buffered saline (PBS) at 37 ºC for 1 hour. The treated cells were lysed with 1.5% sodium dodecyl sulphate (SDS). Cellular fractionation of *S. aureus* cells was performed according to a published protocol (21). Sodium dodecyl sulfate-polyacrylamide gel electrophoresis (SDS-PAGE) was performed to separate the proteins followed by the transfer of proteins to polyvinylidene difluoride membrane. The membrane was incubated with blocking buffer (tris-buffered saline containing 5% skim milk, 25µg/ml Human immunoglobulin G, and 0.2% Tween-20) for 1 hour at room temperature. Antibodies against synthesized peptides (CGSRGLRKKGLRPFR) based on the Cls2 sequence were generated in rabbits by GenScript. DnaK, GroEL and F1β antiserums provided by Professor Trevor Lithgow (22) were raised in rabbits using the yeast mitochondrial homologues and were used as loading controls. Anti-rabbit IgG-peroxidase antibody (Sigma-Aldrich) was used as the secondary antibody followed by the addition of

chemiluminescent substrates. Chemiluminescence was detected using Chemidoc XRS + system (Bio-Rad).

Bodipy-daptomycin staining and super-resolution microscopy

S. aureus strains were grown to mid-exponential phase and incubated with 16 μg/ml Bodipy-fluorescein-labelled daptomycin (courtesy provided by Cubist Pharmaceuticals) following a published protocol (23). The cells were collected by centrifugation to remove excess unincorporated Bodipy-daptomycin followed by resuspension in fresh LB broth. To estimate the amount of Bodipy-daptomycin bound to *S. aureus* strains, the fluorescence intensity of bacterial cells was measured following excitation at 488 nm and emission at 510 nm using a Tecan Infinite M200 plate reader and normalized to whole cell protein contents estimated using the bicinchoninic acid (BCA) protein assay kit (Thermo Scientific) according to a published protocol (24). For imaging using super-resolution microscopy, the cells were imaged using a stimulated emission depletion (STED; Abberior Instruments GmbH, Göttingen, Germany) microscope equipped with an Olympus 100x oil objective (UPlanSApo NA = 1.4) with a 1 watt 595nm pulsed STED laser. Image acquisition was performed with a STED laser power of 40% and 488nm excitation laser power of 10%.

STED images of Bodipy-daptomycin stained *S. aureus* strains were analysed in FIJI by drawing a line around the membrane of each cell to be analysed and then the intensity data extracted and exported as a .csv file. For each cell, the intensity data was sorted to determine the maximum value and then normalised to that value. To interrogate the distribution of membrane fluorescence the process was repeated for all replicates of the strains, the data collected together and a frequency distribution plot generated using Graph Pad Prism 7.0.1. The data was interrogated by one-way ANOVA followed by Dunnett's multiple comparisons test to compare the A8819 and A8819 *cls2* point mutants. A histogram plot of the normalised data was generated to highlight the mean values of the strains.

Detection of muropeptides, lipoteichoic acid, wall teichoic acid, DNA and proteins in purified PG and CL fractions

Purified PG and CL fractions were solubalized in methanol:butanol (1:1(v/v)) with 10 mM ammonium formate and injected into liquid chromatography (Agilent LC1290) coupled with mass spectrometry (Agilent QTOF 6550). Positive and negative modes were used to detect peaks corresponding to muropeptides, lipoteichoic acid and wall teichoic acid based on previous published results (25-27). The purified PG and CL fractions were also processed to produce liposome (1 μg/ μl lipids) in PBS and PCR was performed using Taq (Roche) with primers AP85/AP86 to detect genomic DNA in the liposome suspensions.

FITC-poly-L-lysine binding assay

To investigate differences in bacterial cell surface charge, a FITC-poly-L-lysine binding assay was performed using an established protocol (28). Briefly, overnight cultures of staphylococcal cells were centrifuged and washed with HEPES buffer (20mM, pH 7.5). Cell concentrations were adjusted to an OD_{580} of 0.1 using HEPES buffer. FITC poly-L-lysine was added to the cell suspension to a final concentration of 10μg/ml and incubated for 10 minutes at room temperature. The cells were centrifuged and the fluorescent intensity of FITC poly-L-lysine in the supernatant was measured at 500nm excitation and 530nm emission in a 96 well plate (BD Falcon). The readings were compared to HEPES buffer with or without FITC poly-L-lysine to calculate the amount of FITC poly-L-lysine bound to the cells.

Statistical analysis

Statistics were generated using GraphPad Prism software. The D'Agostino-Pearson omnibus test was used to assess for normal distribution. ANOVA or Kruskal-Wallis test were performed based on the normality of samples followed by pairwise comparisons using Dunnett's, Turkey's, or Dunn's multiple comparison tests. The assumption of similar variances between groups for a one-way ANOVA was justified with the Brown-Forsythe test. Chi-square test for trend was used for comparisons of bacterial burden in zebrafish after infection over time. Student's *t*-tests were performed as unpaired two-tailed analyses. $P < 0.05$ was considered significant for all analyses.

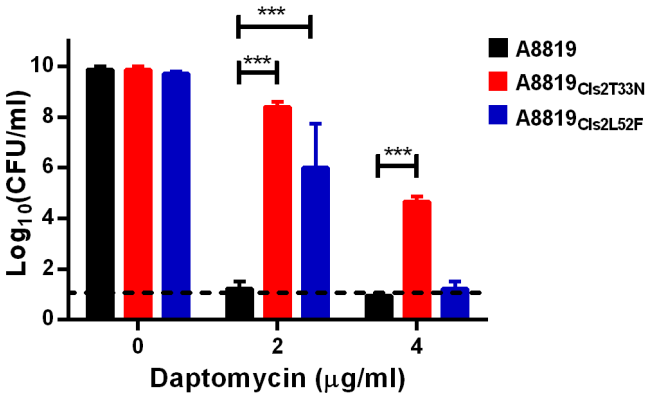

Fig. S1. Daptomycin tolerance of $A8819_{Cls2T33N}$ and $A8819_{Cls2L52F}$. The survival of $A8819_{Cls2T33N}$ and $A8819_{Cls2L52F}$ was measured after exposure to daptomycin for 24 hours. Dashed line indicates the detection limit of 1 $\log_{10}$ CFU/ml. *$P < 0.05$, **$P < 0.01$, ***$P < 0.001$ compared to wild-type A8819 using a one-way ANOVA with Dunnett's multiple comparison test. All experiments were performed three times. Error bars represent mean ± SEM.

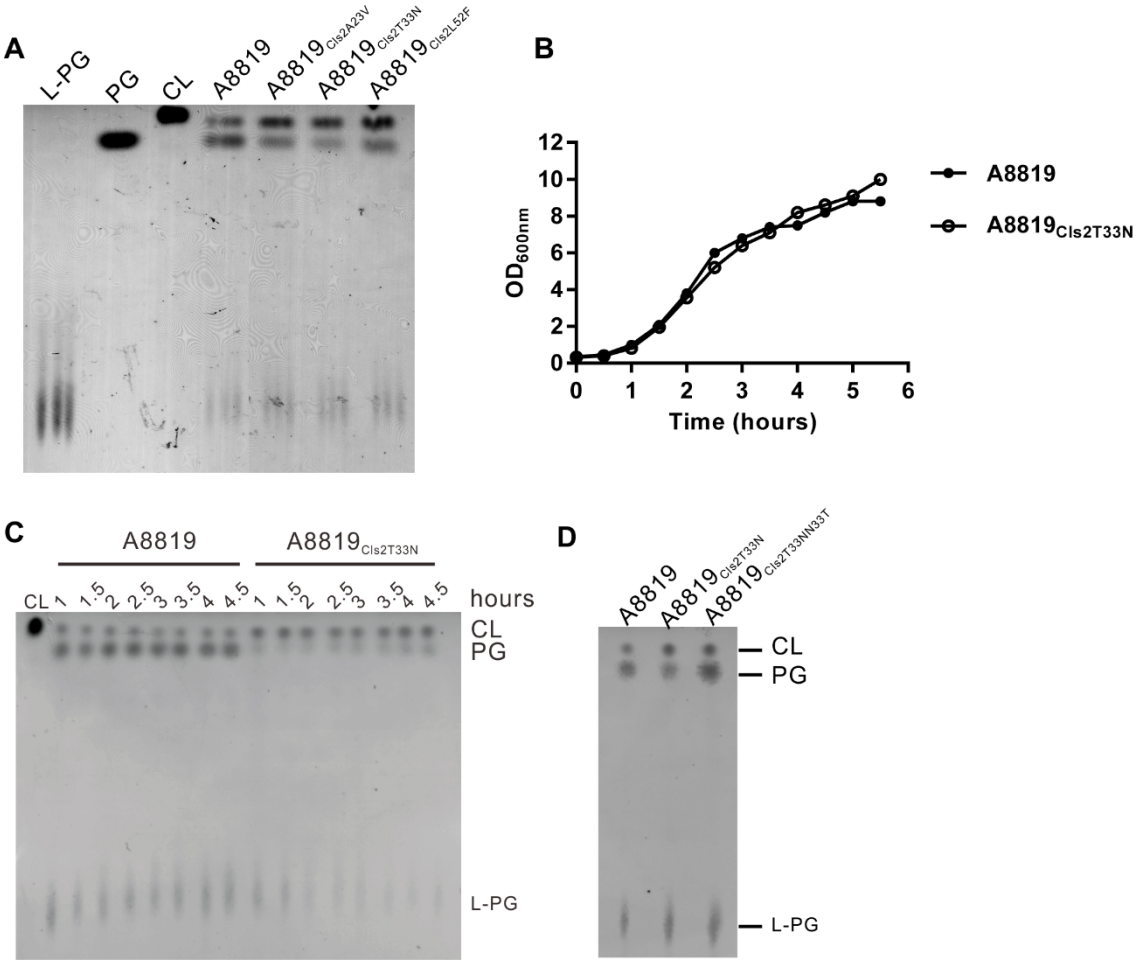

Fig. S2. More CL and less PG were detected in A8819$_{Cls2A23V}$, A8819$_{Cls2T33N}$ and A8819$_{Cls2L52F}$ compared to A8819 using thin layer chromatography (TLC). (*A*) Lipids extracted from A8819$_{Cls2A23V}$, A8819$_{Cls2T33N}$ and A8819$_{Cls2L52F}$ grown to stationary phase were analyzed using TLC. Synthetic CL, PG and L-PG were used as markers as indicated. (*B*) Optical density throughout the bacterial growth of A8819$_{Cls2T33N}$ and A8819. (*C*) Lipids were extracted from the cells at the indicated time in the growth phase and analyzed using TLC. (*D*) Lipids extracted from A8819$_{Cls2T33N}$, A8819$_{Cls2T33NN33T}$ and A8819 were analyzed using TLC.

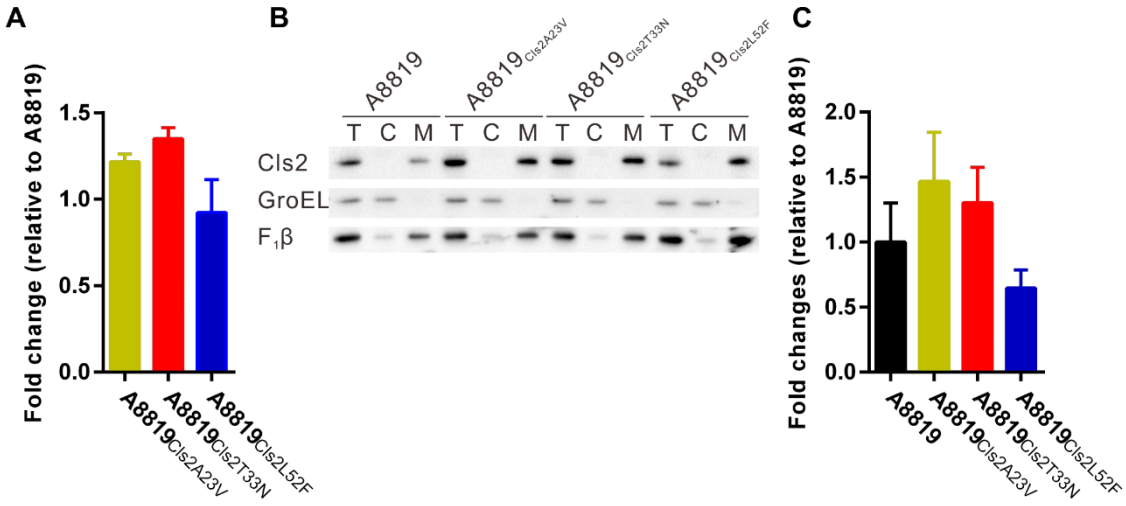

Fig. S3. The levels of *cls2* mRNA and Cls2 protein in A8819$_{Cls2A23V}$, A8819$_{Cls2T33N}$, and A8819$_{Cls2L52F}$ were comparable to that of A8819. (*A*) The expression of *cls2* in A8819$_{Cls2A23V}$, A8819$_{Cls2T33N}$, A8819$_{Cls2L52F}$ and A8819 were measured using quantitative RT-PCR followed by the normalization to 16S rRNA. (*B*) Cells were fractionated to separate cytosoles and membranes followed by the detection of Cls2 using Western blot. GroEL and $F_1\beta$ were used as markers for the cytosolic fraction and membrane fraction, respectively. Representative images were shown. T denotes whole cell lysate, C denotes cytosolic fraction, and M denotes membrane fraction. (*C*) Densitometry was applied to quantify Cls2 detected in (*B*) followed by normalization to the internal control $F_1\beta$. All experiments were performed three times. Error bars represent mean ± SEM. One-way ANOVA followed by Dunnett's multiple comparisons test was used to compare the levels of mRNA or protein between the *cls2* point mutants and A8819. No significant differences were determined.

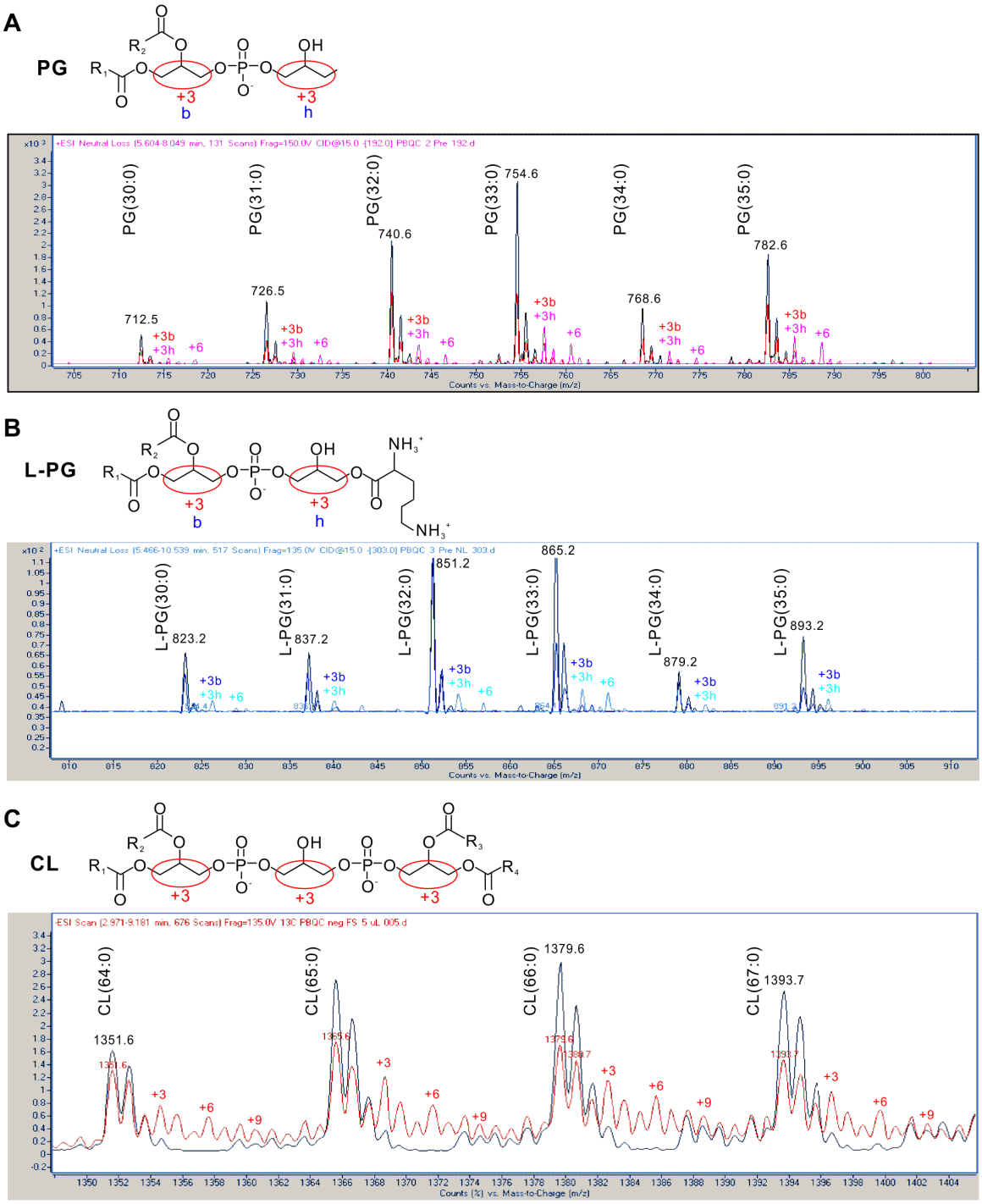

Fig. S4. Detection of *de novo* phospholipid synthesis using mass spectrometry after metabolic labelling with ^{13}C-glycerol. (*A*) ^{13}C-glycerol can be incorporated into PG as the head group (h) or the L-glycerol 3-phosphate backbone (b) as indicated by red ovals. Mass spectrums of precursor 189 scan showed that ^{13}C-glycerol incorporated into PG as the backbone (+3b) (red), whilst the spectrum of precursor 192 scan showed that ^{13}C-glycerol incorporated as the head group (+3h) (pink) or both backbone and head groups (+6) (pink). (*B*) Mass spectrums of neutral loss scan of 300 showed that ^{13}C-glycerol incorporated into L-PG as the backbone (+3b) (blue) whilst neutral loss scan of 303

showed that ^{13}C-glycerol incorporated as the head group (+3h) (cyan) or both backbone and head groups (+6) (cyan). (*C*) Mass spectrums of negative ion mode full scan showed that ^{13}C-glycerol incorporated into CL species (+3, +6 and +9) (red) as indicated. Black spectrums showed in (*A*-*C*) were samples incubated with normal glycerol as negative controls. Numbers represent *m*/*z*.

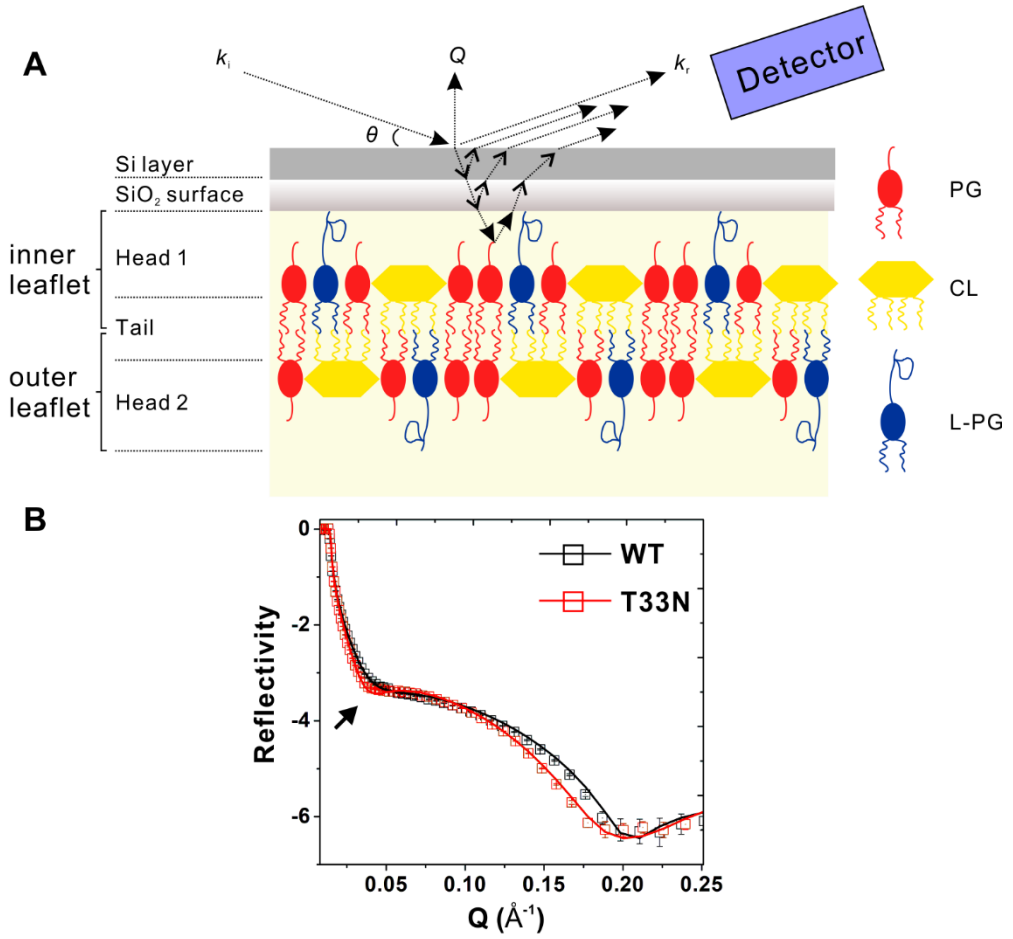

Fig. S5. Structural analysis of clinically relevant *S. aureus* membranes using neutron reflectometry. (*A*) Neutrons probe the molecular structure of a bilayer membrane assembled on a silicon dioxide (SiO_2) surface, including projections into the aqueous layer. The incident neutron is shown as k_i while the reflected beam is indicated as k_r. The angle of the incidence is indicated as θ and is equal to the angle of reflection, and the scattering vector is shown as Q. (*B*) The neutron reflectivity profiles (symbols) and fits (lines) in D_2O of A8819 and $A8819_{Cls2T33N}$ membrane models were retrieved from Fig. 3A and 3B, and overlaid to show the shift of $A8819_{Cls2T33N}$ NR curve (arrow), which corresponds to membrane thickness changes.

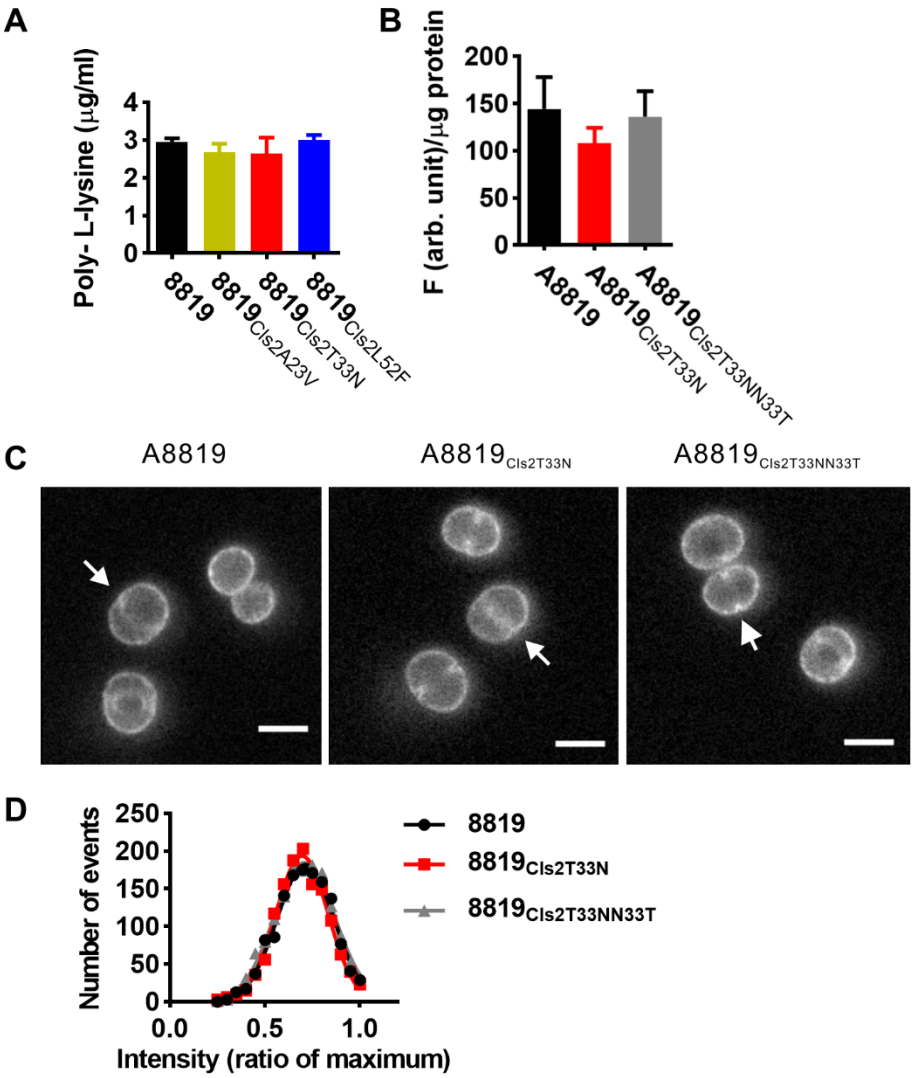

Fig. S6. Characterization of daptomycin binding and cell surface charge. (*A*) Surface charge, as measured by poly-L-lysine binding, of the *cls2* point mutants was similar compared to the parental strain A8819. (*B*) Quantitative assessment of BODIPY-daptomycin binding based on fluorescence intensity (cell number adjusted for by protein content from whole bacterial cells) was similar between $A8819_{Cls2T33N}$ and A8819. (*C*) Representative images from stimulated emission depletion (STED) microscopy of the wild-type (A8819) and point mutant bacterial cells after incubation with BODIPY-daptomycin. Scale bar = 1 μ m. Arrows indicate division septum. (*D*) Fluorescence intensity distribution around cell surface in (*C*) was analysed. Fourteen cells from individual strain were randomly picked for the analysis. Experiments were performed four times for (*A*) and seven times for (*B*). Error bars represent mean ± SEM. One-way ANOVA followed by Dunnett's multiple comparisons test was used to compare the levels of surface charge, BODIPY-daptomycin binding, and fluorescence intensity distribution. No significant differences were determined between the *cls2* point mutants and A8819.

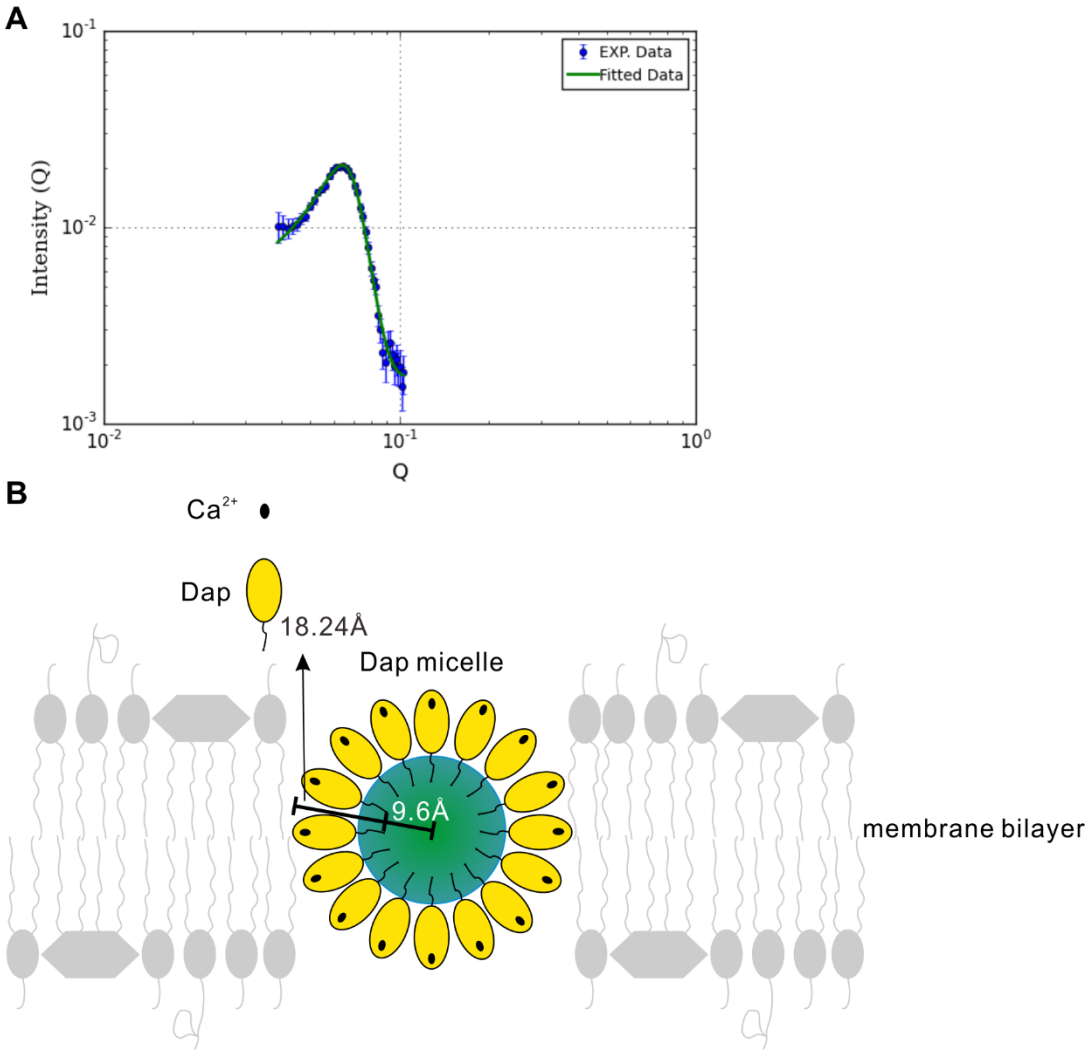

Fig. S7. Daptomycin micelle formation in the A8819 membrane as determined by small-angle neutron scattering. (*A*) The Bragg peak corresponding to the daptomycin micelle (as seen in **Fig. 3E**) was extracted for the calculation of the daptomycin micelle size and subunits using core-shell modelling. (*B*) Schematic illustration of the daptomycin micelle formed within the membrane.

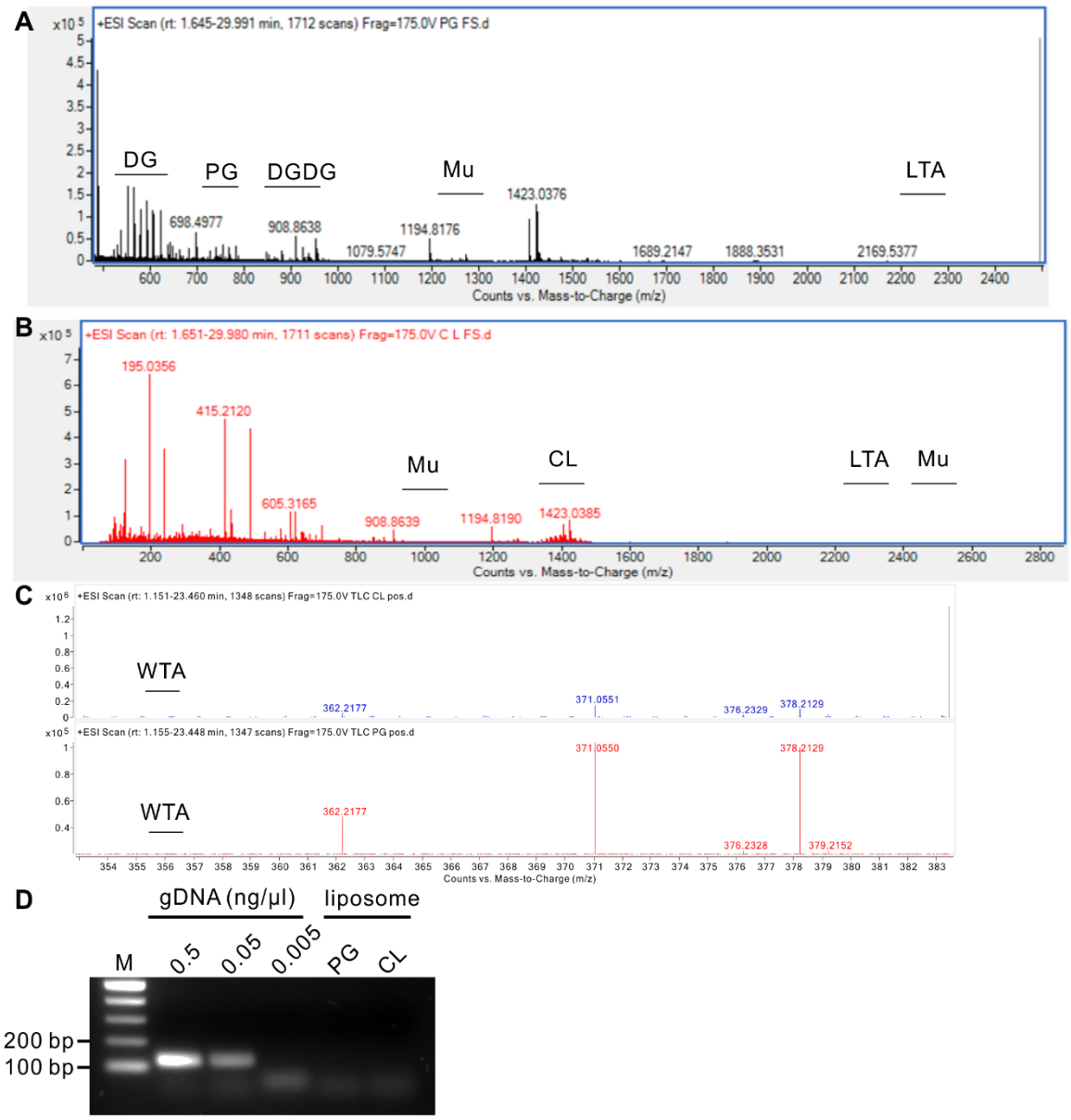

Fig. S8. Mass spectrums of fractions containing PG or CL purified from *S. aureus* A8819 using positive ion mode are shown in (*A*) and (*B*), respectively. (*C*) Mass spectrums of PG fraction (top) and CL fraction (bottom) in the range of 350 to 390 are shown. The numbers indicate *m*/*z*. Peaks corresponding to the molecular species are indicated. DG, diacylglycerol; DGDG, diglycosyldiacylglycerol; Mu, muropeptides; LTA, lipoteichoic acid; WTA, wall teichoic acid. (*D*) Detection of genomic DNA (gDNA) using PCR.

Table S1. Daptomycin susceptibility of *Staphylococcus aureus* strains used in this study

Strain	Description	MIC (μg/ml)
A8819	Daptomycin susceptible clinical isolate (29), wild-type	0.5
$A8819_{Cls2A23V}$	A8819, $Cls2^{A23V}$	0.5 - 1
$A8819_{Cls2T33N}$	A8819, $Cls2^{T33N}$	2
$A8819_{Cls2L52F}$	A8819, $Cls2^{L52F}$	1
$A8819_{Cls2T33NN33T}$	APS169, $Cls2^{N33T}$ (T33N repair)	0.5
A8817	Daptomycin resistant clinical isolate (mutations: $MprF^{T345I}$, $Cls2^{F60S}$, $LeuS^{N468D}$, $MnaA^{R302S}$, IspA truncation) (29)	2
A9744	Daptomycin resistant clinical isolate (mutations: $MprF^{S337L}$, $Cls2^{A23V}$, Atl truncation, AgrC truncation, $Stp1^{M99I}$, $SA1246^{G47E}$) (29)	2
A9764	Daptomycin resistant clinical isolate (mutations: $MprF^{L826F}$, $Cls2^{L52F}$, $SA1667^{L54H}$) (30)	4
A10151	Laboratory-derived daptomycin resistant isolate (mutation: $Cls2^{T33N}$) (29)	4

Table S2. Summary of theoretical neutron scattering length densities of the lipid components, daptomycin and solution subphases.

Lipid/Solvent	Neutron scattering length density (nSLD) (10^{-6} Å^{-2})
D_2O	6.35
H_2O	-0.56
PG head group in D_2O	3.59
PG head group in H_2O	2.78
CL head group in D_2O	3.11
CL head group in H_2O	2.91
L-PG head group in D_2O	3.78
L-PG head group in H_2O	2.02
Head group of wild-type (A8819) membrane (PG:CL:L-PG=69:12:19) in D_2O	3.57
Head group of wild-type (A8819) membrane (PG:CL:L-PG=69:12:19) in H_2O	2.65
Head group of $A8819_{Cls2T33N}$ membrane (PG:CL:L-PG=23:60:17) in D_2O	3.33
Head group of $A8819_{Cls2T33N}$ membrane (PG:CL:L-PG=23:60:17) in H_2O	2.73
CL, PG, and L-PG tails	-0.28
Daptomycin in D_2O	3.96
Daptomycin in H_2O	2.41

Table S3. Substrate and bilayer properties of reconstituted A8819 and $A8819_{Cls2T33N}$ membranes before daptomycin treatment. Error is two standard deviations.

	A8819					$A8819_{Cls2T33N}$				
Layer	Thickness (Å)	nSLD[a] in D_2O / $\times 10^{-6}$ Å^{-2}	nSLD in H_2O / $\times 10^{-6}$ Å^{-2}	V_f[b] of lipid (%)	R[c] (Å)	Thickness (Å)	nSLD in D_2O / $\times 10^{-6}$ Å^{-2}	nSLD in H_2O / $\times 10^{-6}$ Å^{-2}	V_f of lipid (%)	R[d] (Å)
SiO_2	11.6 ± 1.3	3.94 ± 0.23	3.12 ± 0.13	-	1	15.9 ± 0.9	4.46 ± 0.26	2.72 ± 0.10	-	1
HG1[d]	13.7 ± 1.4	4.53 ± 0.36	1.38 ± 0.11	60.5 ± 4.8	1	14.8 ± 1.1	4.66 ± 0.81	1.17 ± 0.20	52.5 ± 8.3	1
Tails	28.1 ± 0.7	0.57 ± 0.03	-0.32 ± 0.02	86.5 ± 0.8	1	28.4 ± 1.2	1.10 ± 0.07	-0.34 ± 0.02	78.5 ± 1.3	1
HG2[d]	7.6 ± 1.2	4.88 ± 0.49	0.92 ± 0.09	46 ± 5.4	1	14.6 ± 1.4	5.35 ± 0.16	0.35 ± 0.02	27.7 ± 2.1	1

a. nSLD, neutron scattering length density, the fitted D_2O SLD is 5.99×10^{-6} Å^{-2} and 6.13×10^{-6} Å^{-2} for A8819 and $A8819_{Cls2T33N}$, respectively.
b. V_f, volume fraction.
c. R, roughness
d. HGs, head groups of inner leaflet (HG1) and outer leaflet (HG2) shown in Fig. S5A.

Table S4. Substrate and bilayer properties of reconstituted A8819 membranes treated with daptomycin. Error is two standard deviations.

Layer	Thickness (Å)	nSLD[a] ($\times 10^{-6}$ Å^{-2})		V_f[b] (%)		R[c] (Å)
		D_2O[d]	H_2O[d]	Lipid	Dp[e]	-
2 µg/ml daptomycin						
SiO_2	11.6 ± 1.3	3.94 ± 0.23	3.12 ± 0.13	-	-	1
HG1[f]	16.2 ± 0.7	5.03 ± 0.24	0.43 ± 0.32	31 ± 10	0	1
Tails	26.2 ± 1.4	1.55 ± 0.09	-0.41± 0.08	71.7 ± 1.5	0	1
HG2[f]	11.9 ± 2.3	5.04 ± 0.12	0.52 ± 0.12	33.6 ± 3.8	0	1
4 µg/ml daptomycin						
SiO_2	11.6 ± 1.3	3.94 ± 0.23	3.12 ± 0.13	-	-	1
HG1[f]	15.5 ± 2.0	4.89 ± 0.25	0.55 ± 0.43	30.3 ± 6.4	4.5 ± 0.1[g]	1
Tails	31.0 ± 1.0	2.63 ± 0.08	-0.21 ± 0.12	52.8 ± 1.3	4.5 ± 0.1	1
HG2[f]	17.1 ± 2.2	4.50 ± 0.23	0.12 ± 0.09	15.8 ± 2.9 (head) 17.2 ± 1.2 (tails)	4.5 ± 0.1[g]	1
Dp layer	20.6 ± 1.3	5.32 ± 0.13	-0.17 ± 0.08	-	17.4 ± 1.9	1
8 µg/ml daptomycin						
SiO_2	11.6 ± 1.3	3.94 ± 0.23	3.12 ± 0.13	-	-	1
HG1[f]	25.2 ± 2.6	5.97 ± 0.10	0.09 ± 0.24	10.5 ± 1.5 (HG + Dp)[g]		1
Tails	27.3 ± 4.2	4.08 ± 0.10	0.08 ± 0.09	26.6 ± 1.6	12.5 ± 1	1
HG2[f]	21.6 ± 2.8	4.81 ± 0.19	0.07 ± 0.09	14.7 ± 0.2 11.9 ± 3.1 (tails)	12.5 ± 1[h]	1
Dp layer	30.8 ± 1.2	5.55 ± 0.09	-0.19 ± 0.14	-	12.6 ± 1.3	1

a. nSLD, neutron scattering length density, the fitted D_2O SLD is 6.01 × 10^{-6} Å^{-2}.
b. V_f, volume fraction.
c. R, roughness
d. Solvent used in the measurement
e. Dp, daptomycin
f. HGs, head groups of inner leaflet (HG1) and outer leaflet (HG2) shown in Fig. S5A.

g. Calculation of daptomycin volume fraction in head region was not achievable as the theoretical SLDs of daptomycin and head group are close.
h. Volume fraction of daptomycin in tail region was used to estimate the daptomycin volume fraction in head group regions.

Table S5. Substrate and bilayer properties of reconstituted $A8819_{Cls2T33N}$ membranes treated with daptomycin. Error is two standard deviations.

Layer	Thickness (Å)	nSLD[a] ($\times 10^{-6}$ Å^{-2})		V_f[b] (%)		R[c] (Å)
		D_2O[d]	H_2O[d]	Lipid	Dp[e]	-
2 µg/ml daptomycin						
SiO_2	15.9 ± 0.9	4.46 ± 0.26	2.72 ± 0.10	-	-	1
HG1[f]	15.6 ± 1.7	5.11 ± 0.21	0.22 ± 0.26	23.7 ± 7.9	0	1
Tails	28.3 ± 1.6	1.83 ± 0.09	-0.21 ± 0.11	66.3 ± 1.4	0	1
HG2[f]	17.8 ± 4.3	4.96 ± 0.16	-0.03 ± 0.09	16 ± 2.8	0	1
4 µg/ml daptomycin						
SiO_2	15.9 ± 0.9	4.46 ± 0.26	2.72 ± 0.10	-	-	1
HG1[f]	16.6 ± 1.1	4.87 ± 0.11	0.30 ± 0.19	26.8 ± 5.9	0	1
Tails	30.3 ± 1.3	2.09 ± 0.07	-0.36 ± 0.09	62 ± 1.1	0	1
HG2[f]	18.4 ± 1.9	4.98 ± 0.35	-0.01 ± 0.10	16.8 ± 2.8	0	1
Dp layer	16.8 ± 4.7	5.36 ± 0.09	-0.49 ± 0.28	-	14.9 ± 1.4	1
8 µg/ml daptomycin						
SiO_2	15.9 ± 0.9	4.46 ± 0.26	2.72 ± 0.10	-	-	1
HG1[f]	15.6 ± 1.9	4.76 ± 0.19	0.22 ± 0.27	23.7 ± 8.2	0	1
Tails	30.8 ± 1.1	2.04 ± 0.07	-0.34 ± 0.10	62.8 ± 1.1	0	1
HG2[f]	19.3 ± 1.6	4.50 ± 0.15	0.03 ± 0.09	17.9 ± 2.8	0	1
Dp layer	31.8 ± 4.5	5.41 ± 0.06	-0.49 ± 0.03	-	14.1 ± 0.9	1

a. nSLD, neutron scattering length density, the fitted D_2O SLD is 5.99×10^{-6} Å^{-2}.
b. V_f, volume fraction.
c. R, roughness
d. Solvent used in the measurement
e. Dp, daptomycin
f. HGs, head groups of inner leaflet (HG1) and outer leaflet (HG2) shown in Fig. S5A.

Table S6. Bacterial strains, plasmids, and oligonucleotides used in this study

Bacterial strain, plasmid, or oligonucleotide	Description (relevant genotype or phenotype) or sequence (5' to 3')	Source, reference or DNA sequence targeted by indicated restriction endonuclease
Escherichia coli strain		
DC10B	Δ*dcm* in DH10B background; Dam methylation only	(1)
Staphylococcus aureus strains		
APS168	$A8819_{Cls2A23V}$, A8819 with Cls2 A23V substitution	This study
APS169	$A8819_{Cls2T33N}$, A8819 with Cls2 T33N substitution	This study
APS170	$A8819_{Cls2L52F}$, A8819 with Cls2 L52F substitution	This study
APS218	$A8819_{Cls2T33NN33T}$, APS169 with Cls2 N33T substitution	This study
APS171	APS168 with pALC2084	This study
APS172	APS169 with pALC2084	This study
APS173	APS170 with pALC2084	This study
APS232	APS218 with pALC2084	This study
APS281	A8819 with pALC2084	This study
Plasmids		
pIMAY	Plasmid with *E.coli* replicon and temperature-sensitive Gram-positive replicon; tetracycline inducible secY antisense; Cm^r	This study
pAP87	pIMAY with *cls2* loci from A8817, generated with oligonuleotides AP529, AP382, AP383 and AP515	This study
pAP88	pIMAY with *cls2* loci from A9744, generated with oligonuleotides AP529, AP382, AP383 and AP515	This study
pAP89	pIMAY with *cls2* loci from A10151, generated with oligonuleotides AP529, AP382, AP383 and AP515	This study
pAP90	pIMAY with *cls2* loci from A9764, generated with oligonucleotides AP529, AP382, AP383 and AP515	This study
pALC2084	pALC2073 with *gfp* cloned into the EcoRI site	(18)
Oligonucleotides		
AP85	GACATGGGTTCTCGTGGACT	
AP86	TCGATGGTTTCGATTGTTCA	
AP151	GGCAAGCGTTATCCGGAATT	
AP152	GTTTCCAATGACCCTCCACG	
AP382	ATTACGGATATCTTGTATTAGGTCA	EcoRV
AP383	CTAATACAAGATATCCGTAATGCTA	EcoRV
AP515	GCAAGCGGCCGCACGGATGGTCAGGTTTATTAG	NotI
AP517	GCAAGTCGACCCATCTAATAAGATTAGCTGCG	SalI

AP529	GCAAGTCGACTCACCTCGTTTGGATCGCTTT	SalI
AP352 (IM151)	TACATGTCAAGAATAAACTGCCAAAGC	(1)
AP353 (IM152)	AATACCTGTGACGGAAGATCACTTCG	(1)

References

1. Monk IR, Shah IM, Xu M, Tan MW, & Foster TJ (2012) Transforming the untransformable: application of direct transformation to manipulate genetically Staphylococcus aureus and Staphylococcus epidermidis. *mBio* 3(2).
2. CLSI (2014) *Performance Standards for Antimicrobial Susceptibility Testing; Twenty-Fourth Informational Supplement. CLSI document M100-S24.* (Clinical and Laboratory Standards Institute).
3. Yang SJ, Mishra NN, Rubio A, & Bayer AS (2013) Causal role of single nucleotide polymorphisms within the mprF gene of Staphylococcus aureus in daptomycin resistance. *Antimicrobial agents and chemotherapy* 57(11):5658-5664.
4. Tsai M*, et al.* (2011) Staphylococcus aureus requires cardiolipin for survival under conditions of high salinity. *BMC microbiology* 11:13.
5. Hu C*, et al.* (2008) RPLC-ion-trap-FTMS method for lipid profiling of plasma: method validation and application to p53 mutant mouse model. *Journal of proteome research* 7(11):4982-4991.
6. Clifton LA*, et al.* (2015) Effect of divalent cation removal on the structure of gram-negative bacterial outer membrane models. *Langmuir : the ACS journal of surfaces and colloids* 31(1):404-412.
7. James M*, et al.* (2011) The multipurpose time-of-flight neutron reflectometer "Platypus" at Australia's OPAL reactor. *Nuclear Instruments and Methods in Physics Research Section A* 632(1):112-123.
8. Nelson A (2010) Motofit – integrating neutron reflectometry acquisition, reduction and analysis into one, easy to use, package. *Journal of Physics: Conference Series* 251(1):012094.
9. Nelson A (2006) Co-refinement of multiple-contrast neutron/X-ray reflectivity data using MOTOFIT. *Journal of Applied Crystallography* 39:273-276.
10. Heinrich F*, et al.* (2009) A new lipid anchor for sparsely tethered bilayer lipid membranes. *Langmuir : the ACS journal of surfaces and colloids* 25(7):4219-4229.
11. Holt SA*, et al.* (2009) An ion-channel-containing model membrane: structural determination by magnetic contrast neutron reflectometry. *Soft Matter* 5(13):2576-2586.
12. Gilbert EP, Schulz JC, & Noakes TJ (2006) 'Quokka'—the small-angle neutron scattering instrument at OPAL. *Physica B* 385-386:1180-1182.
13. Kline SR (2006) Reduction and Analysis of SANS and USANS Data using Igor Pro. *Journal of Appled Crystallography* 39(6):895-900.
14. Ilavsky J & Jemian PR (2009) Irena: tool suite for modeling and analysis of small-angle scattering. *Journal of Appled Crystallography* 42(2):347-353.
15. Guinier A FG (1955) *Small angle scattering of X-rays* (John Wiley & Sons. Inc); trans Wilson C. B.
16. Hall C, Flores MV, Storm T, Crosier K, & Crosier P (2007) The zebrafish lysozyme C promoter drives myeloid-specific expression in transgenic fish. *BMC developmental biology* 7:42.
17. Bhuiyan MS*, et al.* (2016) Acinetobacter baumannii phenylacetic acid metabolism influences infection outcome through a direct effect on neutrophil chemotaxis.

Proceedings of the National Academy of Sciences of the United States of America 113(34):9599-9604.
18. Bateman BT, Donegan NP, Jarry TM, Palma M, & Cheung AL (2001) Evaluation of a tetracycline-inducible promoter in Staphylococcus aureus in vitro and in vivo and its application in demonstrating the role of sigB in microcolony formation. *Infection and immunity* 69(12):7851-7857.
19. Corriden R*, et al.* (2008) Ecto-nucleoside triphosphate diphosphohydrolase 1 (E-NTPDase1/CD39) regulates neutrophil chemotaxis by hydrolyzing released ATP to adenosine. *The Journal of biological chemistry* 283(42):28480-28486.
20. Hope MJ, Bally MB, Webb G, & Cullis PR (1985) Production of large unilamellar vesicles by a rapid extrusion procedure: characterization of size distribution, trapped volume and ability to maintain a membrane potential. *Biochimica et biophysica acta* 812(1):55-65.
21. Frankel MB, Wojcik BM, DeDent AC, Missiakas DM, & Schneewind O (2010) ABI domain-containing proteins contribute to surface protein display and cell division in Staphylococcus aureus. *Molecular microbiology* 78(1):238-252.
22. Clements A*, et al.* (2009) The reducible complexity of a mitochondrial molecular machine. *Proceedings of the National Academy of Sciences of the United States of America* 106(37):15791-15795.
23. Dhand A*, et al.* (2011) Use of antistaphylococcal beta-lactams to increase daptomycin activity in eradicating persistent bacteremia due to methicillin-resistant Staphylococcus aureus: role of enhanced daptomycin binding. *Clinical infectious diseases : an official publication of the Infectious Diseases Society of America* 53(2):158-163.
24. Tran TT*, et al.* (2013) Daptomycin-resistant Enterococcus faecalis diverts the antibiotic molecule from the division septum and remodels cell membrane phospholipids. *mBio* 4(4).
25. Hewelt-Belka W*, et al.* (2014) Comprehensive methodology for Staphylococcus aureus lipidomics by liquid chromatography and quadrupole time-of-flight mass spectrometry. *Journal of chromatography. A* 1362:62-74.
26. Ornelas-Soares A*, et al.* (1993) The peptidoglycan composition of a Staphylococcus aureus mutant selected for reduced methicillin resistance. *The Journal of biological chemistry* 268(35):26268-26272.
27. Eugster MR & Loessner MJ (2011) Rapid analysis of Listeria monocytogenes cell wall teichoic acid carbohydrates by ESI-MS/MS. *PloS one* 6(6):e21500.
28. Mukhopadhyay K*, et al.* (2007) In vitro susceptibility of Staphylococcus aureus to thrombin-induced platelet microbicidal protein-1 (tPMP-1) is influenced by cell membrane phospholipid composition and asymmetry. *Microbiology* 153(Pt 4):1187-1197.
29. Peleg AY*, et al.* (2012) Whole genome characterization of the mechanisms of daptomycin resistance in clinical and laboratory derived isolates of Staphylococcus aureus. *PloS one* 7(1):e28316.
30. Hayden MK*, et al.* (2005) Development of Daptomycin resistance in vivo in methicillin-resistant Staphylococcus aureus. *Journal of clinical microbiology* 43(10):5285-5287.